Combustion Theory and Modelling
Vol. 10, No. 2, April 2006, 199–217

Taylor & Francis
Taylor & Francis Group

Operator-splitting with ISAT to model reacting flow with detailed chemistry

M. A. SINGER*†, S. B. POPE‡ and H. N. NAJM§

†Center for Applied Mathematics, Cornell University, Ithaca, NY, USA
‡Sibley School of Mechanical and Aerospace Engineering,
Cornell University, Ithaca, NY, USA
§Combustion Research Facility, Sandia National Laboratories,
Livermore, CA, USA

(Accepted August 2005)

We further increase the computational performance of an operator-split projection scheme for the solution of the equations governing reacting flows with detailed chemistry. This enhancement is achieved by using *in situ* adaptive tabulation (ISAT) to compute the pure reaction sub-steps; the treatment of diffusion and convection is unchanged. The modified scheme is applied to an unsteady one-dimensional laminar premixed methane–air flame problem using detailed GRIMech3.0 chemical kinetics. For this problem we demonstrate second-order temporal convergence, investigate the impact of the ISAT error tolerance on solution accuracy, and compare results with and without ISAT. Computational performance is also examined where we observe a reaction sub-step speed-up factor due to ISAT of approximately 13; the overall time step speed-up is approximately 7.5. Extension of the scheme to multiple dimensions is discussed.

Keywords: Operator splitting; ISAT; projection; tabulation; flame

1. Introduction

The direct numerical simulation (DNS) of turbulent reacting flows is a computationally challenging task which requires considerable computing power. Among the reasons for such high demands on computing resources is the requirement that DNS resolve completely all of the length scales in a turbulent flow. For engineering scale flows with Reynolds numbers of the order 10^5, this means finely spaced grids are required to discretize the governing equations. In addition to turbulence resolution, the presence of chemical reactions also contributes to the computational expense. The accurate modeling of combustion processes using detailed reaction mechanisms introduces stiff systems of differential equations which must be solved. Further, the combustion chemistry can also introduce length scales smaller than the Kolmogorov turbulence length scale: these scales must be resolved adequately. As a result, the development of numerically efficient DNS algorithms which reduce the demands on computational resources is necessary to allow DNS to be applied to a greater range of problems.

*Corresponding author. E-mail: singer@cam.cornell.edu

Combustion Theory and Modelling
ISSN: 1364-7830 (print), 1741-3559 (online)
http://www.tandf.co.uk/journals
DOI: 10.1080/13647830500307501

The present work describes the incorporation of *in situ* adaptive tabulation (ISAT) [1] into the algorithm of Najm and Knio [2] so as to reduce significantly the computational cost of reacting flow computations. ISAT is a storage/retrieval procedure which works in conjunction with an ordinary differential equation (ODE) integrator to solve the evolution equations for an adiabatic, isobaric mixture: the mixture composition changes solely as a result of chemical reactions. Therefore, to account numerically for mixture composition changes due to convection and diffusion, an operator-splitting numerical approach which separates species evolution due to transport from changes due to chemical reaction is most natural. The operator-split projection scheme of [2] does just that. Developed in the context of the low Mach number reacting flow equations, this scheme has been used for simulating one- and two-dimensional laminar flames; the same methodologies and framework, however, can also be applied to the fully compressible flow equations in the context of DNS of turbulent flames. The scheme separates chemical species diffusion from species reaction while treating convection explicitly; the scheme serves as the base algorithm into which we insert ISAT. Due to the use of operator-splitting, the incorporation of ISAT into this scheme involves only modification of the chemical reaction sub-steps: the remainder of the algorithm is unchanged.

In addition to ISAT, other computational methods are used to reduce the computational cost of solving the equations governing combustion chemistry. In [3], for example, the Flame Prolongation of ILDM (FPI) model was used to describe premixed, partially premixed, and diffusion combustion. Alternatively, an adaptive chemistry approach was taken in [4] wherein different chemical kinetics models were used in different regions of the computational domain. The Piecewise Reusable Implementation of Solution Mapping (PRISM) [5, 6] method is also used to reduce the computational cost of reacting flow computations. In [7], for example, PRISM was applied in adaptive turbulent premixed flame calculations.

In recent years, operator-splitting schemes have been used in a variety of scientific applications including reacting flow simulations. In [8] and [9], for example, operator-splitting is used to separate chemical reaction processes from transport processes in atmospheric modeling simulations. Schwer *et al.* [10] also used an operator-split scheme to study an H_2/O_2 burner flame and three partially premixed laminar methane flames using detailed chemistry. Their work also examined the accuracy and effectiveness of operator-split methods for computing steady-state reacting flows. In [11], Najm and Wyckoff constructed a second-order predictor-corrector projection scheme to solve the two-dimensional low Mach number reacting flow equations. Their scheme was then extended to an additive semi-implicit projection scheme [12]: a stiff, operator-split construction then followed [13]. Most recently, the scheme has seen performance enhancements and the incorporation of detailed transport models [2]. Day and Bell [14] have used operator-splitting in the context of an adaptive projection scheme for low Mach number reacting flows. Their scheme has been applied to such areas as steady and unsteady methane diffusion flames [14], three-dimensional premixed turbulent methane flames [15], and Type 1a supernovae [16].

ISAT has been used beneficially in conjunction with operator-splitting schemes. Yang and Pope [17], for example, used operator-splitting in the context of PDF calculations of turbulent reacting flows. Their work showed that an operator-split formulation coupled with ISAT can speed-up PDF calculations by a factor of 100–1000 over the use of direct integration. Further, Singer and Pope [18] used ISAT with Strang splitting for unsteady one-dimensional calculations corresponding to a constant density and constant molecular diffusivity laminar flame: an ISAT speed-up factor around 5 was observed. ISAT has yet to be applied to the DNS of reacting flows.

In section 2 we review briefly the low Mach number conservation equations and the assumptions underlying the present formulation. Section 3 describes the numerical scheme used to solve these governing equations. We begin by reviewing the operator-split construction

in [2] and then describe the modifications made to the original scheme to allow ISAT to be used; additional remarks follow. Section 4 presents computational results obtained using the modified splitting scheme with ISAT. These results are based on a one-dimensional laminar methane–air flame problem which includes detailed chemical kinetics. This problem serves as a test case for demonstrating the temporal convergence and accuracy of the scheme: two- and three-dimensional unsteady flame calculations, for which such studies are too expensive computationally, are of primary interest and will be studied in subsequent work. However, because the modifications of the algorithm discussed here pertain only to the time-stepping portion of the scheme and are unrelated to the spatial differencing, the one-dimensional problem serves as an adequate test. A detailed study of spatial convergence and accuracy of the original scheme is found in [13]. Finally, in section 5 we summarize and draw final conclusions.

2. Governing equations

The transport equations used here to model reactive flow are identical to those used in [11] for the original scheme formulation. We now briefly review the underlying assumptions and state the governing equations.

The model assumes an ideal gas mixture with zero bulk viscosity. Soret and Dufour effects, external body forces, and radiant heat transfer are neglected. The governing equations are based on the zero Mach number limit of the compressible conservation equations [19, 20]. In this limit, the detailed effects of acoustic waves are ignored while still allowing for large heat release, significant variations in density and temperature, and the interaction of combustion with the hydrodynamic flow field [20]. For the problems considered in this work, the computational domains have boundaries open to the atmosphere.

Based on the assumptions above, the non-dimensional equations governing the conservation of mass, momentum, energy, and chemical species are:

$$\frac{\partial \rho}{\partial t} + \nabla \cdot (\rho \mathbf{u}) = 0, \tag{1}$$

$$\frac{\partial (\rho \mathbf{u})}{\partial t} + \nabla \cdot (\rho \mathbf{u}\mathbf{u}) = -\nabla p + \frac{1}{\mathrm{Re}} \mathbf{\Phi}, \tag{2}$$

$$\frac{\partial T}{\partial t} + \mathbf{u} \cdot \nabla T = \frac{1}{\mathrm{Re}\,\mathrm{Pr}} \frac{\nabla \cdot (\lambda \nabla T)}{\rho c_p} + \frac{1}{\mathrm{Re}\,\mathrm{Sc}} \frac{\mathbf{Z} \cdot \nabla T}{c_p} + \mathrm{Da} \frac{\omega_T}{\rho c_p}, \tag{3}$$

$$\frac{\partial (\rho Y_i)}{\partial t} + \nabla \cdot (\rho \mathbf{u} Y_i) = \frac{1}{\mathrm{Re}\,\mathrm{Sc}} \nabla \cdot (\rho Y_i \mathbf{V}_i) + \mathrm{Da}\, \omega_i, \tag{4}$$

respectively. Here, ρ is the density, $\mathbf{u}$ is the velocity vector, p is the hydrodynamic pressure, $\mathbf{\Phi}$ is the divergence of the viscous stress tensor, T is the temperature, λ is the thermal conductivity, ω_T is the rate of heat release, Y_i is the mass fraction of species i, ω_i is the net chemical production rate of species i, and

$$c_p = \sum_{i=1}^{n_s} Y_i c_{p,i}, \tag{5}$$

is the mixture specific heat where n_s is the number of chemical species and $c_{p,i}$ is the specific heat at constant pressure of species i. The constants Re, Pr, Sc, and Da are the Reynolds, Prandtl, Schmidt, and Damköhler numbers, respectively.

The conservation equations above are supplemented with the equation of state

$$P_0 = \rho T / W, \tag{6}$$

where P_0 is the constant thermodynamic pressure and $W \equiv 1/\sum_{i=1}^{n_s} Y_i/W_i$ is the local effective molar mass of the mixture; W_i is the molecular weight of species i.

As in [12, 13], we use Fick's first law of diffusion which relates the diffusive flux of species i to its mass fraction gradient [21]. Then, we use the approximation that the n_s-th chemical species, taken to be N_2, dominates the mixture characteristics such that the binary diffusion velocity of any other species $i \neq n_s$ in the mixture is approximated by

$$\mathbf{V}_i = -\frac{1}{Y_i}\mathcal{D}_{in_s}\nabla Y_i, \quad i = 1, 2, \ldots, n_s - 1, \tag{7}$$

where $\mathcal{D}_{in_s}$ is the binary mass diffusion coefficient of species i into N_2 at the local temperature and pressure of the mixture. Finally, we define $\mathbf{Z} \equiv -\sum_{i=1}^{n_s} c_{p,i} Y_i \mathbf{V}_i = \sum_{i=1}^{n_s} c_{p,i}\mathcal{D}_{in_s}\nabla Y_i$ where again use is made of Fick's law for expressing the diffusion velocity in terms of the mass fraction gradient. For computational efficiency, the mixture transport properties μ and λ are set to those of N_2 at the local temperature [12]. All of the assumptions described above are consistent with those used in [12, 13] to construct the original splitting scheme; they are summarized here for completeness. Finally, we note that use of detailed transport models (e.g. mixture-averaged) is necessary for more realistic computations.

3. Numerical scheme

In this section, we describe the numerical scheme used to discretize the low Mach number equations. In section 3.1 we review the original operator-split scheme of [2] into which ISAT is incorporated. Then, in section 3.2 we describe in detail how ISAT is incorporated into the original operator-split scheme. Finally, in section 3.3 we provide some additional remarks regarding the formulation and implementation of the scheme.

For notational convenience, the equations are expressed as follows

$$\frac{\partial(\rho Y_i)}{\partial t} = C_i + D_i + R_i, \tag{8}$$

$$\frac{\partial \rho}{\partial t} = C_\rho + D_\rho + R_\rho, \tag{9}$$

$$\frac{\partial(\rho \mathbf{u})}{\partial t} = \mathbf{N}(\rho, \mathbf{u}) + \mathbf{F}(\mu, \mathbf{u}) - \nabla p, \tag{10}$$

where

$$C_i \equiv -\nabla\cdot(\rho \mathbf{u} Y_i), \quad D_i \equiv \frac{1}{\mathrm{Re}\,\mathrm{Sc}}\nabla\cdot(\rho\mathcal{D}_{in_s}\nabla Y_i), \quad R_i \equiv \mathrm{Da}\,\omega_i, \tag{11}$$

$$C_\rho \equiv \frac{\rho}{T}\mathbf{u}\cdot\nabla T + W\sum_{i=1}^{n_s}\frac{\rho\mathbf{u}\cdot\nabla Y_i}{W_i}, \tag{12}$$

$$R_\rho \equiv -\frac{1}{c_p T}\mathrm{Da}\,\omega_T - W\sum_{i=1}^{n_s}\mathrm{Da}\frac{\omega_i}{W_i}, \tag{13}$$

$$D_\rho \equiv -\frac{1}{\mathrm{Re}\,\mathrm{Pr}\,c_p T}\nabla\cdot(\lambda\nabla T) + \frac{\rho}{T}\frac{1}{c_p \mathrm{Re}\,\mathrm{Sc}}\mathbf{Z}\cdot\nabla T - \frac{W}{\mathrm{Re}\,\mathrm{Sc}}\sum_{i=1}^{n_s}\frac{\nabla\cdot(\rho\mathcal{D}_{in_s}\nabla Y_i)}{W_i}, \tag{14}$$

and the convective and viscous terms of the momentum equation are denoted by $\mathbf{N}(\rho, \mathbf{u})$ and $\mathbf{F}(\mu, \mathbf{u})$, respectively. To obtain equation (9) for the time evolution of density, we first

differentiate the equation of state with respect to time. Then, equations (3) and (4) are substituted for the temperature and species mass fraction time derivatives, respectively.

3.1 *Existing operator-splitting scheme*

The numerical algorithm summarized here follows closely the operator-split formulation of Najm and Knio [2]. The scheme combines a predictor/corrector construction with a Strang splitting procedure which solves the above described conservation equations by separating the diffusion terms from the reaction terms.

For the predictor portion of the algorithm, the convection terms in the species and density equations are evaluated explicitly using a second-order Adams-Bashforth (AB2) scheme:

$$C_i^e = \frac{3}{2}C_i^n - \frac{1}{2}C_i^{n-1}, \tag{15}$$

$$S_\rho^e = \frac{3}{2}C_\rho^n - \frac{1}{2}C_\rho^{n-1}. \tag{16}$$

The diffusion sub-steps are integrated using a stabilized Runge–Kutta–Chebyshev (RKC) method [22]. The equations governing the reaction sub-steps are

$$\frac{\mathrm{d}(\rho Y_i)}{\mathrm{d}t} = R_i + \frac{1}{2}C_i^e, \tag{17}$$

$$\frac{\mathrm{d}\rho}{\mathrm{d}t} = R_\rho + \frac{1}{2}S_\rho^e, \tag{18}$$

$$T = \frac{P_0 W}{\rho}, \tag{19}$$

and these equations are integrated using the ODE integration package DVODE [24].

Following the Strang-based splitting predictor stage of the scheme is a non-stiff corrector phase which is required for the stability of the variable-density projection scheme [11] and allows for the stable treatment of flows with large density variations [13].

3.2 *Incorporation of ISAT*

Starting from an intial state of the composition specified by $\{\mathbf{Y}, T, P_0\}$ and a time increment Δt, ISAT computes the state of the composition after a time Δt. This new state is obtained by solving the equations governing a homogeneous, adiabatic, isobaric system of n_s chemical species

$$\frac{\mathrm{d}Y_i}{\mathrm{d}t} = \frac{R_i}{\rho}, \tag{20}$$

$$\frac{\mathrm{d}\rho}{\mathrm{d}t} = R_\rho, \tag{21}$$

and the ideal gas constraint (equation (6)).

To use ISAT for the reaction sub-steps of the original scheme, we manipulate equations (17)–(19) into a form which is solved using ISAT. This is done by first writing the reaction sub-step equations in the following form:

$$\frac{\mathrm{d}(\rho Y_i)}{\mathrm{d}t} = \left(\frac{1}{2}C_i^e - Y_i R_\rho\right) + [Y_i R_\rho + R_i], \tag{22}$$

$$\frac{\mathrm{d}\rho}{\mathrm{d}t} = \left(\frac{1}{2}S_\rho^e\right) + [R_\rho], \tag{23}$$

$$T = \frac{P_0 W}{\rho}. \tag{24}$$

As in the original scheme, this system of equations is integrated over a time step Δt. Here, however, we incorporate ISAT by applying a second Strang splitting procedure as follows:

S1. The terms in parentheses ( ) in equations (22) and (23) are integrated over $\Delta t/2$ by solving

$$\frac{\mathrm{d}\left(\rho^{(a)}Y_i^{(a)}\right)}{\mathrm{d}t} = \frac{1}{2}C_i^e - Y_i^{(a)}R_\rho^{(a)}, \tag{25}$$

$$\frac{\mathrm{d}\rho^{(a)}}{\mathrm{d}t} = \frac{1}{2}S_\rho^e, \tag{26}$$

and the ideal gas equation of state. Here, $R_\rho^{(a)}$ denotes R_ρ evaluated using the state of the system determined by $\{\rho^{(a)}, \mathbf{Y}^{(a)}, T^{(a)}\}$. The initial condition is taken to be the final system state from the previous diffusion sub-step. This non-stiff system of equations is integrated over $\Delta t/2$ using a standard second-order, single-stage Runge–Kutta (RK2) scheme.

S2. The remaining terms in square brackets [ ] in equations (22) and (23) are re-expressed as

$$\frac{\mathrm{d}Y_i^{(b)}}{\mathrm{d}t} = \frac{R_i^{(b)}}{\rho}, \tag{27}$$

$$\frac{\mathrm{d}\rho^{(b)}}{\mathrm{d}t} = R_\rho^{(b)}, \tag{28}$$

and are integrated over a full time step, Δt: the equation of state is used to determine the temperature of the system. Here again, $R_i^{(b)}$ denotes R_i evaluated using the state of the system determined by $\{\rho^{(b)}, \mathbf{Y}^{(b)}, T^{(b)}\}$. The initial conditions correspond to the final state of the system from the previous sub-step, $\{\rho^{(a)}(\frac{\Delta t}{2}), \mathbf{Y}^{(a)}(\frac{\Delta t}{2}), T^{(a)}(\frac{\Delta t}{2})\}$. This system of equations is exactly that given by equations (20) and (21): the equations solved by ISAT. Hence ISAT is used to solve the equations above. The resulting mass fractions and density are used to compute the temperature; the new state of the system is $\{\rho^{(b)}(\Delta t), \mathbf{Y}^{(b)}(\Delta t), T^{(b)}(\Delta t)\}$.

S3. A sub-step identical to **S1** is performed taking as the initial conditions the final state of the system from **S2**, $\{\rho^{(b)}(\Delta t), \mathbf{Y}^{(b)}(\Delta t), T^{(b)}(\Delta t)\}$. At the completion of this sub-step, the final state of the system is given by $\{\rho^{(c)}(\frac{\Delta t}{2}), \mathbf{Y}^{(c)}(\frac{\Delta t}{2}), T^{(c)}(\frac{\Delta t}{2})\}$. This serves as the initial condition for the next Strang diffusion sub-step in the original scheme.

3.3 *Additional remarks*

3.3.1 Temporal accuracy. With DVODE used for calculation of the reaction sub-steps, the original scheme described above is second-order accurate in time [2]. In the present work, the incorporation of ISAT is performed in a manner designed to preserve the second-order convergence rate of the scheme. In particular, we use second-order accurate Strang sub-splitting and a second-order Runge–Kutta scheme. The test problem and associated results described below demonstrate that second-order temporal accuracy is indeed preserved.

3.3.2 Strang sub-splitting. As noted above, the second splitting procedure (Strang sub-splitting) is necessary in order to manipulate the density and species mass fraction equations

into a form which can be solved using existing ISAT libraries. The first and last sub-steps involve systems of non-stiff ODEs which are integrated using a second-order Runge–Kutta scheme. The use of RK2 preserves the overall second-order temporal accuracy of the scheme while requiring only two source term evaluations per sub-step; the source terms for the density equation are constant and pre-computed at the beginning of each time step. Finally, we note that the pure reaction sub-steps contain all of the stiffness due to the chemical reaction source terms; these equations are solved using ISAT.

3.3.3 Spatial discretization. For the current implementation of the algorithm described above, spatial gradients are approximated using second-order centered finite differences. Near domain boundaries, these differences are evaluated using ghost cells which lie outside of the computational domain. These extra cells are necessary for proper implementation of the boundary conditions and maintain the overall second-order spatial accuracy of the scheme.

3.3.4 Scheme stability. The numerical stability of the scheme without ISAT is discussed extensively in [2, 11–13]. Here we summarize by remarking that the corrector portion of the algorithm enhances the coupling between the density, velocity, and hydrodynamic pressure fields thereby contributing to the overall stability of the scheme [11]. In addition, due to the extended stability region of the RKC scheme, integration of the diffusion sub-steps can be performed with larger global integration time steps than usable by treating the diffusion terms using an explicit multistep scheme. Further, as discussed in [2], RKC requires fewer computationally expensive source term evaluations and hence exhibits a significant computational speed-up in comparison to an explicit multistep scheme.

The inclusion of ISAT for computing the reaction sub-steps does not alter the stability characteristics of the reaction portion of the algorithm. The two RK2 sub-steps of the Strang sub-splitting procedure do, however, impose stability restrictions on Δt. These constraints on Δt are less restrictive then those due to diffusion processes and hence are not found to impact the overall stability of the scheme.

4. Results

We examine the accuracy and performance characteristics of the predictor/corrector splitting scheme and its use of ISAT. To do so, we consider a one-dimensional freely propagating laminar premixed methane–air flame at atmospheric pressure. This test problem is used for accuracy and convergence studies of the original scheme [2, 12, 13] and serves as an application on which the scheme modifications are thoroughly tested within a reasonable amount of CPU time: applications of greater spatial complexity (i.e. two- and three-dimensional) are expected to exhibit similar temporal characteristic since scheme modifications are confined to the time-stepping portion of the algorithm. For the problem considered here, the fresh unburnt gas is a stoichiometric mixture of methane and air at 300 K and 1 atm pressure. For the combustion chemistry we use GRImech3.0 [26] which consists of 53 species and 325 reversible chemical reactions. The number of RKC diffusion and momentum stages are set to $S = 8$ and $L = 4$, respectively. A more complete discussion of the impact of S and L on scheme accuracy and convergence is found in [2].

The dynamic viscosity (μ), thermal conductivity (λ), and diffusion coefficients ($\mathcal{D}_{in_s}$) are pre-computed using Chemkin [27, 28] and tabulated as functions of temperature; transport quantities used in the calculations are then computed from table values using linear

interpolation. As used in [12, 13], all tables have a temperature increment of $\Delta T = 0.01$ K. The tables containing μ and λ have approximately 24,000 entries while the table containing $\mathcal{D}_{in_s}$ has approximately 24,000 entries per species. This approach to computing the transport properties speeds the calculations while maintaining the spatial and temporal accuracy of the scheme [13]. Since the primary purpose of the test problem is to demonstrate scheme convergence, accuracy, and performance, the use of tabulated transport properties is sufficient for the present study. It should be noted, however, that use of detailed transport models will affect the overall CPU time and could impact the performance of the scheme.

To begin the calculations, a freely propagating stoichiometric premixed methane–air flame with the above chemical mechanism is first computed using Chemkin in one spatial dimension. The steady-state solution is then interpolated onto a uniform one-dimensional grid and used as the initial condition for the computations. We consider the computational domain having 512 grid points in $x \in [0, 0.8]$ cm with outflow boundary conditions. In a reference frame fixed on the computational domain, the flame propagates from right to left. Initially, the flow exhibits a period of unsteady propagation as the flame structure, position, and reactions rates adjust to the spatial grid discretization and transport coefficients used in the present code; these are different than those used by Chemkin to obtain the initial flame profile. Following this period of unsteadiness, the flame propagates with a constant speed—the laminar flame speed. For the results shown below the flame remains sufficiently far from the computational boundaries so that boundary effects are minimal.

In section 4.1 we show steady-state flame profiles which demonstrate the qualitative nature of the solutions. Section 4.2 examines the accuracy and convergence of the scheme and demonstrates the consistency of the ISAT scheme with the DVODE scheme. In section 4.3 we examine the impact of the ISAT error tolerance on solution accuracy. DVODE and ISAT results are compared thoroughly in section 4.4 and computational performance is discussed in section 4.5. Finally, section 4.6 provides further discussion regarding the scheme and its implementation.

4.1 *Solution profiles*

The qualitative nature of the solution is examined by viewing species and temperature profiles. Figure 1 shows steady-state flame profiles at time $t \approx 3.8 \times 10^{-5}$ s; all initial transients have disappeared and the flame continues to propagate with this profile until it reaches the left-end of the computational domain. The figure demonstrates qualitatively expected behavior as indicated by comparing the profiles with other work [13, 30].

To quantify numerically our spatial grid resolution in relation to the flame width, we characterize the width of the flame by

$$\delta_L \equiv \frac{T_b - T_u}{\max(|\mathrm{d}T/\mathrm{d}x|)}, \tag{29}$$

where T_b and T_u are the burnt and unburnt mixture temperatures, respectively [11]. Using this expression and the profile data from Figure 1 we obtain $\delta_L \approx 4.16 \times 10^{-2}$ cm. Given that the spatial resolution is $\Delta x = 0.8\,\mathrm{cm}/512 \approx 1.56 \times 10^{-3}$ cm, we note that there are approximately 26 grid points in the flame; a sufficient number to resolve completely the flame structure.

4.2 *Temporal convergence*

In this section we examine the temporal convergence properties of the scheme. Before beginning, however, we note that the originally constructed scheme which uses DVODE for the

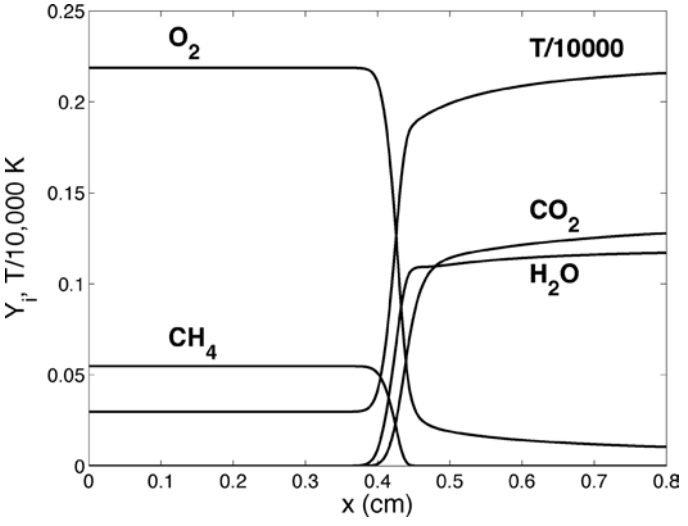

Figure 1. Steady-state solution profiles of major species mass fractions and temperature at time $t \approx 3.8 \times 10^{-5}$ s. Ambient temperature reactants are on the left and hot combustion products are on the right.

reaction sub-steps [2] is second-order accurate in Δt. This convergence rate was demonstrated for both self-convergence of the scheme (differences of numerically obtained field quantities using successively higher temporal resolution) and cross-convergence of the scheme (error in the splitting scheme in relation to a non-split formulation).

All of the results for this convergence study are obtained at time $t \approx 3.8 \times 10^{-5}$ s. To ensure that temporal errors are dominant over ISAT tabulation and ODE integration errors, we set the ISAT error tolerance to $\varepsilon_{\text{tol}} = 1 \times 10^{-10}$ and the absolute and relative ODE integrator error tolerances to $\varepsilon_{\text{abs}} = \varepsilon_{\text{rel}} = 10^{-10}$. A more complete discussion of the ISAT error tolerance is found in section 4.3. We present below convergence results for $\{T, u, \rho, Y_{\text{CH}_4}, Y_{\text{HCO}}, Y_{\text{CH}}\}$. The former three quantities are selected due to their fundamental importance to the flow; the latter three are selected as important major and minor species and are those studied in [2]. The HCO radical, for example, is the best marker of heat release from the flame for a stoichiometric premixed methane flame [29]. Similar convergence results are observed for other major and minor species.

To examine the self-convergence of the scheme, we define the normalized self-convergence RMS error as

$$\varepsilon_{\Delta t}^{\text{self}} = \frac{\left\| \theta_{\Delta t}^{\text{ISAT}} - \theta_{\Delta t/2}^{\text{ISAT}} \right\|}{\left\| \theta_{\Delta t_s}^{\text{ISAT}} \right\|}, \tag{30}$$

where θ is any field quantity (e.g. temperature, velocity) and the subscripts denote the associated temporal resolution. The notation $\theta_{\Delta t_s}^{\text{ISAT}}$ is used to denote field quantities computed using the ISAT scheme with a small value of Δt: $\Delta t_s \approx 2.13 \times 10^{-8}$ s. The norm notation refers to the standard 2-norm over space (i.e. the root mean square over the grid nodes). We use $\varepsilon_{\Delta t}^{\text{self}}$ to measure the amount of temporal discretization error present in solutions with successively smaller Δt; $\varepsilon_{\Delta t}^{\text{self}} = \mathcal{O}(\Delta t^2)$ then implies second-order temporal accuracy. Figure 2 plots $\varepsilon_{\Delta t}^{\text{self}}$ as a function of Δt. The symbols denote numerically obtained quantities while the solid lines are of slope two.

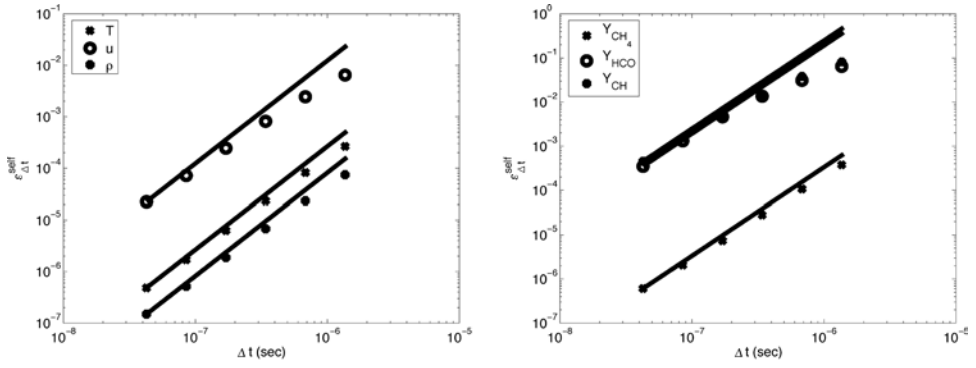

Figure 2. Self-convergence of $\varepsilon_{\Delta t}^{\text{self}}$ as defined by equation (30) plotted against Δt for the ISAT splitting scheme at $t \approx 3.8 \times 10^{-5}$ s. The ISAT error tolerance is $\varepsilon_{\text{tol}} = 1 \times 10^{-10}$ and the absolute and relative ODE integrator error tolerances are $\varepsilon_{\text{abs}} = \varepsilon_{\text{rel}} = 10^{-10}$. The symbols represent numerically obtained results and the solid lines shown for reference have slope two.

Cross-convergence of the ISAT scheme in relation to an accurate DVODE solution is demonstrated in figure 3 by defining the normalized cross-convergence RMS error as

$$\varepsilon_{\Delta t}^{\text{cross}} = \frac{\left\| \theta_{\Delta t}^{\text{ISAT}} - \theta_{\Delta t_s}^{\text{DVODE}} \right\|}{\left\| \theta_{\Delta t_s}^{\text{DVODE}} \right\|}, \tag{31}$$

where Δt_s is a small time step used to obtain an accurate DVODE solution. In this case, $\Delta t_s \approx 1.07 \times 10^{-8}$ s which is one-quarter the smallest ISAT step size shown in figure 3. For the DVODE calculations, the absolute and relative ODE integrator error tolerances are set to 10^{-8} and 10^{-14}, respectively. These values are consistent with those used for convergence studies in [2]. In figure 3, the symbols denote numerically obtained quantities while the solid lines are lines of slope two. We observe clearly that the results from the ISAT scheme converge to the DVODE results second-order in Δt.

We conclude from the results above that the incorporation of ISAT via the Strang sub-splitting approach preserves the second-order temporal convergence of the scheme. We also note that, as demonstrated in figure 3, for $\Delta t \lesssim 2 \times 10^{-7}$ s there is less than one percent error between the ISAT and DVODE solutions for the quantities shown.

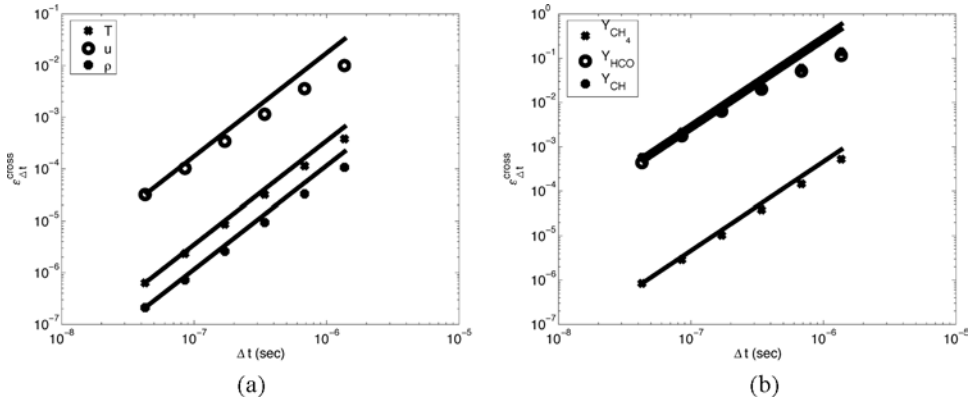

Figure 3. Cross-convergence of $\varepsilon_{\Delta t}^{\text{cross}}$ as defined by equation (31) against time step for the ISAT splitting scheme in relation to the original DVODE splitting scheme at time $t \approx 3.8 \times 10^{-5}$ s.

4.3 *Impact of the ISAT error tolerance*

The ISAT error tolerance, ε_{tol}, is a user-specified local error tolerance which determines whether or not a given query composition is sufficiently close to a composition for which the reaction mapping has been computed and tabulated. If it is, then a relatively inexpensive ISAT table retrieve is performed to compute the reaction mapping; otherwise, DI is performed and an EOA is grown or a new entry is added to the ISAT table. Therefore, to minimize computational cost we wish to maximize ε_{tol} while still maintaining specified accuracy of the flame solution. In this section we investigate the impact of ε_{tol} on solution accuracy and determine a value appropriate for further study in the remaining sections. It should be emphasized that increasing ε_{tol} knowingly increases the amount of error (relative to using DI) in the solution. But, as will be demonstrated, this error can be controlled and lowered to an acceptable level by adjusting ε_{tol}.

For all of the calculations in this section, we set the absolute and relative ISAT ODE solver tolerances to $\varepsilon_{\text{abs}} = \varepsilon_{\text{rel}} = 10^{-10}$. Where DVODE calculations are performed, the DVODE absolute and relative error tolerances are set to $\varepsilon_{\text{abs}} = 10^{-8}$ and $\varepsilon_{\text{rel}} = 10^{-14}$, respectively. Therefore, at a given instant in time any given field quantity, ξ, is a function of x, Δt, and ε_{tol}. That is, $\xi = \xi(x, \Delta t, \varepsilon_{\text{tol}})$.

To quantify errors due to temporal discretization and ISAT tabulation, it is necessary to obtain numerically accurate solutions with which to compare. We define here the values of Δt and ε_{tol} used to compute these accurate solutions: $\Delta t = \Delta t_s \equiv 2.27 \times 10^{-8}$ s and $\varepsilon_{\text{tol}} = \varepsilon_{\text{tol}_s} \equiv 1 \times 10^{-12}$. Based on the temporal convergence studies presented earlier, solutions computed with $\Delta t = \Delta t_s$ contain minimal temporal discretization error (less than 0.05% relative to an accurate DVODE solution). When $\varepsilon_{\text{tol}} = \varepsilon_{\text{tol}_s}$, nearly all of the ISAT composition queries are satisfied via DI; very few table retrieves are performed and the resulting ISAT table grows in entries rapidly. It should be noted that, in addition to being highly accurate, solutions obtained using $\Delta t = \Delta t_s$ and $\varepsilon_{\text{tol}} = \varepsilon_{\text{tol}_s}$ are expensive computationally to obtain. Finally, unless otherwise specified, we fix $\Delta t = 1.82 \times 10^{-7}$ s.

We quantify the impact of ε_{tol} on solution accuracy in two ways. First, at a given instant in time and for a fixed value of Δt, we define the normalized RMS error

$$\varepsilon_1^{\text{isat}}(\varepsilon_{\text{tol}}) \equiv \frac{\|\xi(x, \Delta t, \varepsilon_{\text{tol}}) - \xi(x, \Delta t, \varepsilon_{\text{tol}_s})\|}{\|\xi(x, \Delta t, \varepsilon_{\text{tol}_s})\|}, \tag{32}$$

where the norms are 2-norms over the spatial coordinate. Therefore, $\varepsilon_1^{\text{isat}}$ measures the amount of solution error relative to a solution with a small ISAT error tolerance. Figure 4a plots $\varepsilon_1^{\text{isat}}$

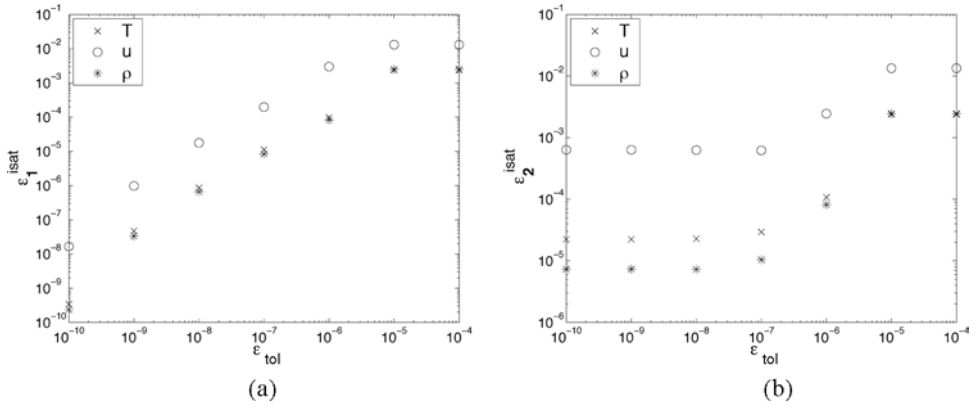

Figure 4. Impact of the ISAT error tolerance, ε_{tol}, on solution accuracy. Results are shown at time $t \approx 8.25 \times 10^{-5}$ s using $\Delta t = 1.82 \times 10^{-7}$ s. (a) The error defined by equation (32), (b) the error defined by equation (33).

as a function of ε_{tol} at $t \approx 8.25 \times 10^{-5}$ s for the temperature, velocity, and density; similar results are also observed for species mass fractions (not shown). We note from the figure that, as anticipated, $\varepsilon_1^{\text{isat}} \to 0$ as $\varepsilon_{\text{tol}} \to 0$ indicating that, for a given Δt, decreasing ε_{tol} decreases the tabulation error introduced by ISAT; more precisely, $\varepsilon_1^{\text{isat}}$ varies linearly with ε_{tol}. If ε_{tol} is made sufficiently small (corresponding to more direct integrations and fewer table retrieves), then the tabulation error is eliminated. We also observe from figure 4a that, for $\varepsilon_{\text{tol}} = 1 \times 10^{-7}$, the temperature, velocity, and density errors are less than 0.07%. Corresponding species errors (not shown) are found to be less than 0.005%.

The second measure of error used to quantify the impact of ε_{tol} on solution accuracy is defined by

$$\varepsilon_2^{\text{isat}}(\varepsilon_{\text{tol}}) \equiv \frac{\|\xi(x, \Delta t, \varepsilon_{\text{tol}}) - \xi(x, \Delta t_s, \varepsilon_{\text{tol}_s})\|}{\|\xi(x, \Delta t_s, \varepsilon_{\text{tol}_s})\|}. \tag{33}$$

In contrast to equation (32), $\varepsilon_2^{\text{isat}}$ measures the error relative to a solution obtained using small values of Δt and ε_{tol} namely $\Delta t = \Delta t_s$ and $\varepsilon_{\text{tol}} = \varepsilon_{\text{tol}_s}$. Therefore, $\varepsilon_2^{\text{isat}}$ characterizes the combination of tabulation and temporal errors. Figure 4b plots $\varepsilon_2^{\text{isat}}$ as a function of ε_{tol}. We observe from the figure that $\varepsilon_2^{\text{isat}}$ is nearly constant for $\varepsilon_{\text{tol}} \leq 1 \times 10^{-7}$; ε_{tol} is sufficiently small so that temporal discretization errors dominate. Here again we observe that, for $\varepsilon_{\text{tol}} = 1 \times 10^{-7}$, temperature, velocity, and density errors are less than 0.02%. Corresponding species errors are found to be less than 0.005%. In addition to the results shown in figure 4b, we further take as 'exact' solutions ξ obtained using DVODE and $\Delta t = \Delta t_s$. These results are nearly identical to those shown in Figure 4b and hence have been omitted.

In comparing figures 4a and b, we note that for $\varepsilon_{\text{tol}} = 1 \times 10^{-7}$ we have $\varepsilon_1^{\text{isat}} \approx \varepsilon_2^{\text{isat}}$ indicating that the ISAT tabulation and temporal discretization errors are comparable in size. For this reason, as well as the small percent errors noted above, we select $\varepsilon_{\text{tol}} = 1 \times 10^{-7}$ for further study.

4.4 *Comparison of DVODE and ISAT results*

In this section we give a detailed comparison of results obtained using the DVODE and ISAT versions of the algorithm. Throughout, based on previous discussion, we set $\Delta t = 1.82 \times 10^{-7}$ s. For the case of ISAT, we set $\varepsilon_{\text{tol}} = 1 \times 10^{-7}$ and the ODE error tolerances to $\varepsilon_{\text{abs}} = \varepsilon_{\text{rel}} = 10^{-10}$. For the calculations involving DVODE, we set the absolute and relative error tolerances to 10^{-6}. This is the value used in [2] for calculations not involving convergence testing. We compare results after approximately 50,000 time steps when $t \approx 9.1 \times 10^{-3}$ s. At this time the flame has propagated approximately 7 flame-widths yet remains well-removed from the left-end boundary of the computational domain.

4.4.1 Laminar flame speeds. We define the absolute laminar flame speed, s_a, as the speed of the flame front relative to a fixed reference frame [31]. This locally determined quantity is computed for the two schemes by plotting the spatial location of the 1400 K isotherm as a function of time; the slope of the resulting line (not shown) is the absolute laminar flame speed. We observe excellent flame front location (and consequently absolute laminar flame speed) agreement between the DVODE and ISAT calculations. Figure 5 shows s_a (computed as the slope of the line connecting the starting flame location and the flame locations at subsequent times) as a function of time. From figure 5 we observe that the absolute speeds of the flames computed by the two schemes demonstrate the same qualitative behavior and are in excellent quantitative agreement. At the final time shown in the figures, $t \approx 9.1 \times 10^{-3}$ s, the DVODE

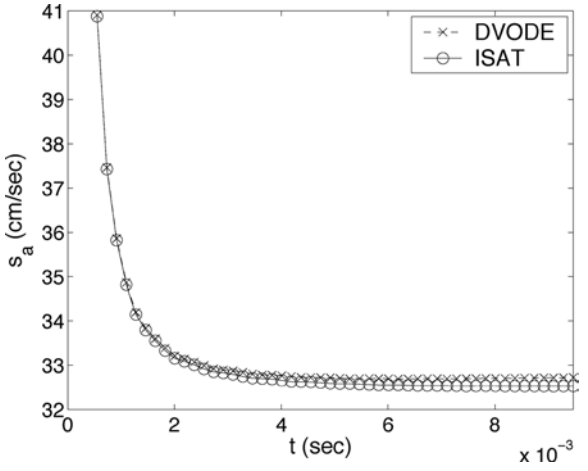

Figure 5. Absolute laminar flame speed, s_a, as a function of time computed by the DVODE and ISAT schemes.

scheme gives $s_a \approx 32.72$ cm/s and the ISAT scheme gives $s_a \approx 32.53$ cm/s; the difference is approximately 0.58%.

To explore further the laminar flame speed, we define the consumption speed

$$s_c = -\frac{1}{\rho_u Y_F^u} \int_{-\infty}^{\infty} \omega_F \, \mathrm{d}x, \tag{34}$$

where ρ_u is the density of the unburnt mixture, Y_F^u is the unburnt fuel mass fraction, and ω_F is the net fuel production rate [32]. This globally determined quantity measures the speed at which the flame burns the reactants and is based only on reaction rates. Figure 6 shows s_c as a function of time for the two schemes. We observe from the figure that the flame speeds from both schemes start off around 36.5 cm/s and then decrease until they reach the steady-state value. From the figure we note that in the steady-state, s_c is greater for the DVODE scheme than for the ISAT scheme. At $t \approx 9.1 \times 10^{-3}$ s the consumption flame speed from DVODE is $s_c \approx 33.19$ cm/s; the corresponding ISAT speed is $s_c \approx 33.17$ cm/s. Hence the DVODE and ISAT speeds differ by approximately 0.06%.

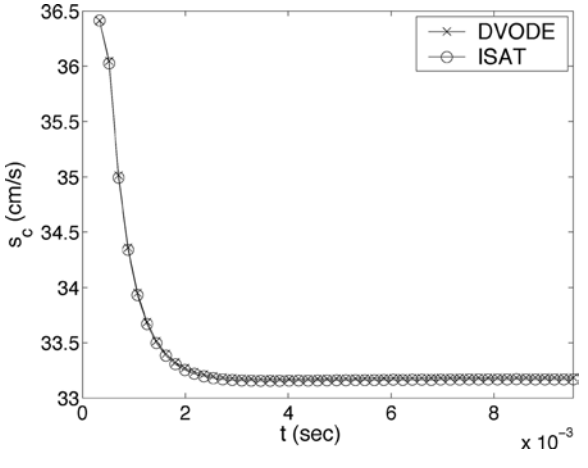

Figure 6. Consumption speed, defined by equation (34), as a function of time for the DVODE and ISAT schemes. The elapsed time between sample points (each symbol in the figure) is $t \approx 1.82 \times 10^{-4}$ s (1000 time steps).

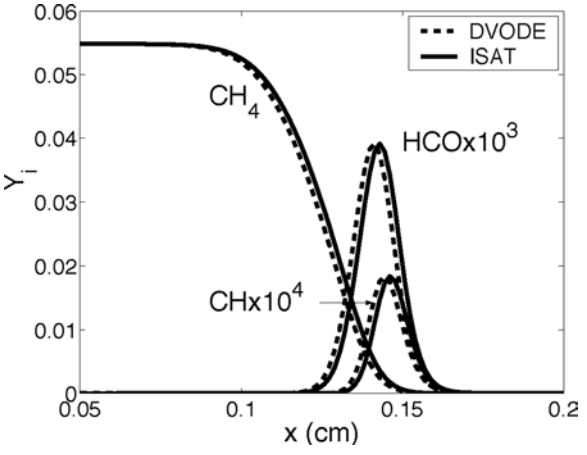

Figure 7. Comparison of DVODE and ISAT species mass fraction profiles (Y_i) for CH_4, HCO, and CH at $t \approx 9.1 \times 10^{-3}$ s (approximately 50, 000 time steps).

The discrepancies in the laminar flame speeds described above are due predominantly to residual ISAT and Δt errors. As demonstrated in section 4.3, the ISAT errors can be reduced by decreasing ε_{tol}. The errors in Δt can be reduced by decreasing Δt.

4.4.2 Species profiles. We examine and compare species profiles (Y_i) from the DVODE and ISAT schemes at time $t \approx 9.1 \times 10^{-3}$ s. Due to the small differences in the velocity fields described above, the profiles from the two schemes are slightly shifted in space relative to each other; this difference in flame location is approximately 0.53% of the total distance traveled. Qualitatively and quantatively, the DVODE and ISAT results are in excellent agreement. As an illustration, Y_i for CH_4, HCO, and CH (the same species used for convergence studies in section 4.2) are shown in figure 7: only the region of the computational domain containing the flame front is shown. For illustration purposes, the HCO and CH mass fraction profiles are scaled by 10^3 and 10^4, respectively. The dashed lines represent DVODE results while the solid lines represent ISAT results. We observe from the figure that all corresponding DVODE and ISAT profiles have similar widths and maximum peak values; the slight difference in flame location is the most obvious discrepancy.

4.5 *Computational performance*

Having demonstrated the accuracy of the ISAT splitting scheme in previous sections, we examine here its computational performance in comparison to the DVODE splitting scheme. We use the same parameter settings as in section 4.4 and run the simulations until $t \approx 9.1 \times 10^{-3}$ s (approximately 50,000 time steps). All calculations are performed using a single R10000 processor running at 195 MHz on a SGI Origin 2000: memory constraints are not a limiting factor.

Figures 8a and b plot the CPU time taken per time step to execute different portions of the algorithm as a function of simulation time. In particular, the following CPU times are shown: time to complete the overall time steps; time spent in the reaction sub-steps; and, time spent in the diffusion sub-steps (RKC). From figure 8a we observe that the DVODE CPU time increases with simulation time. This result is due to the fact that as the flame propagates, species are convected and diffused thereby increasing the portion of the domain containing a mixture of product gases; less of the domain is occupied by pure reactants. Due to the presence

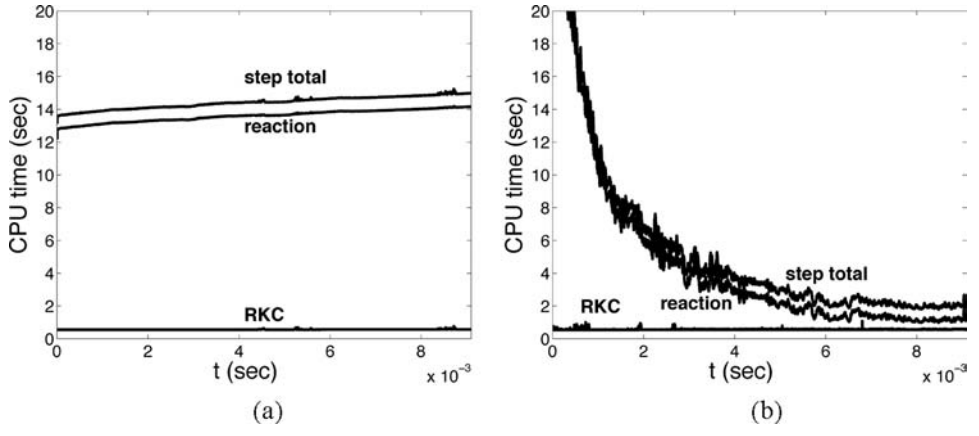

Figure 8. CPU time per time step of the DVODE and ISAT splitting schemes. (a) The DVODE splitting scheme, (b) the ISAT splitting scheme with $\varepsilon_{\text{tol}} = 1 \times 10^{-7}$.

of active chemical processes in these mixtures, it takes DVODE more time steps and Jacobian evaluations to integrate the governing equations; consequently, more CPU time is required to compute the reaction portion of the algorithm. For the DVODE calculations, we also note that the majority of the CPU time per time step is spent in the reaction sub-steps. Approximately 90–95% of the total step time is spent computing the combustion chemistry with the bulk of the remaining time being spent in the RKC update.

In contrast, figure 8b shows the corresponding CPU times for the ISAT algorithm. Here we observe that the overall CPU time decreases with simulation time. Initially, the CPU time required per time step by the ISAT scheme is greater than the time taken by DVODE. During this initial start-up period, most of the CPU time is spent performing computationally expensive direct integrations and EOA grows; additional CPU time is also spent constructing and building the ISAT table. As simulation time elapses and the number of ISAT queries increases, more queries are satisfied by table retrieves which are less expensive computationally than DI; this transition from primarily ISAT adds and grows to ISAT retrieves reduces significantly the CPU time per time step. For $t \gtrsim 7 \times 10^{-3}$ s, most composition queries are satisfied by table retrieves and the per-step CPU times level-off. At this stage of the calculations, the reaction and diffusion sub-steps take approximately the same amount of CPU time per time step.

Figures 9a and b show where the reaction sub-step time is spent. From figure 9a we observe that for the DVODE calculations, nearly all of the reaction sub-step CPU time is spent performing integration of the species and density equations using DVODE. For the case of the ISAT scheme, during the ISAT table construction phase the bulk of the CPU time is spent in ISAT computing the reaction mapping via direct integration; the majority of the remaining reaction sub-step time is spent in the RK2 sub-steps. After the ISAT table is constructed and populated so that most composition queries are satisfied by table retrieves, approximately equal time is spent in ISAT and RK2. To illustrate further the initial table build-up process, figure 10 shows the number of ISAT table retrieves, grows, and additions as a function of the number of ISAT queries. Initially (i.e. for the first six queries), all ISAT queries are satisfied by direct integration as shown in the figure. After approximately 150 queries, however, the majority of events are ISAT retrieves. For the entire calculation which consists of nearly 50,000 time steps, approximately 3×10^7 ISAT queries are made; approximately 97% are satisfied by ISAT retrieves, 2.95% by ISAT grows, and 0.024% by ISAT adds (direct integration).

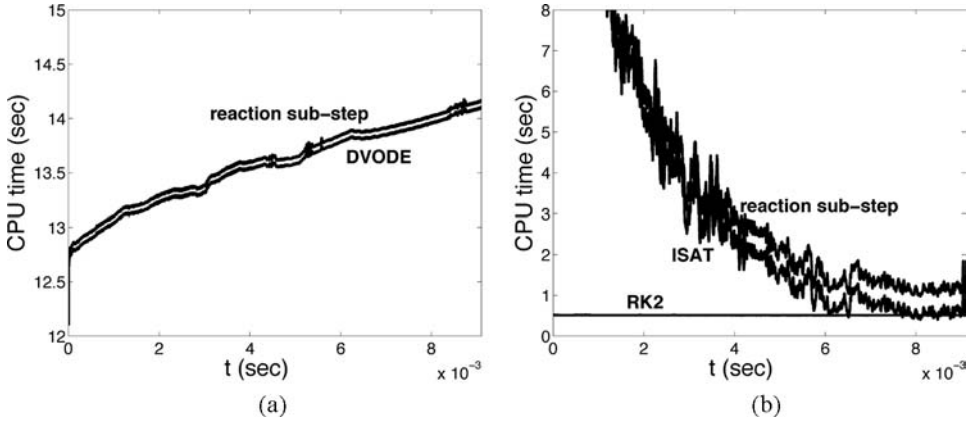

Figure 9. A detailed break-down of the CPU time spent in the reaction sub-steps. (a) DVODE scheme, (b) ISAT scheme with $\varepsilon_{\text{tol}} = 1 \times 10^{-7}$.

To examine further the computational savings of the ISAT scheme, figures 11a and b show the computational speed-up factor as a function of simulation time, where the speed-up factor is defined as

$$\text{speed-up factor} \equiv \frac{\text{CPU time per time step using DVODE scheme}}{\text{CPU time per time step using ISAT scheme}}. \tag{35}$$

Figure 11a shows the speed-up factor for the overall scheme time step. Here we observe that, initially, the speed-up is less than one indicating that the DVODE scheme consumes less CPU time than the ISAT scheme as discussed earlier. Subsequently, the speed-up factor is greater than one indicating that ISAT consumes less CPU time than DVODE. Therefore, following an initial table build-up, the DVODE scheme requires approximately 7–8 times more CPU time per time step than the ISAT scheme. Figure 11b shows the speed-up for the reaction sub-steps of the algorithm. Here we observe similar behavior as in figure 11a with the post-ISAT table

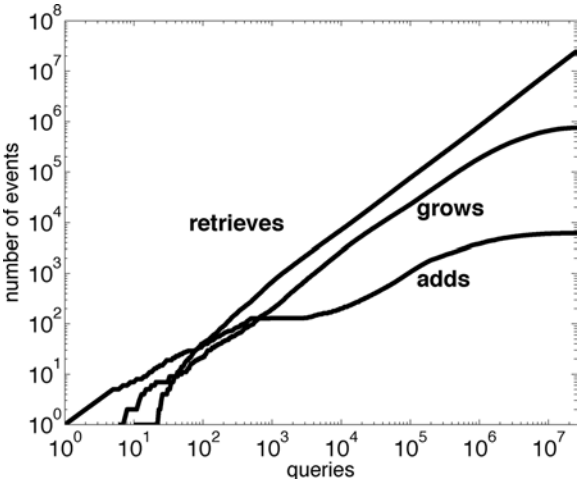

Figure 10. The number of ISAT retrieves, grows, and additions as a function of the number of ISAT queries. The simulation is run for approximately 50,000 time steps.

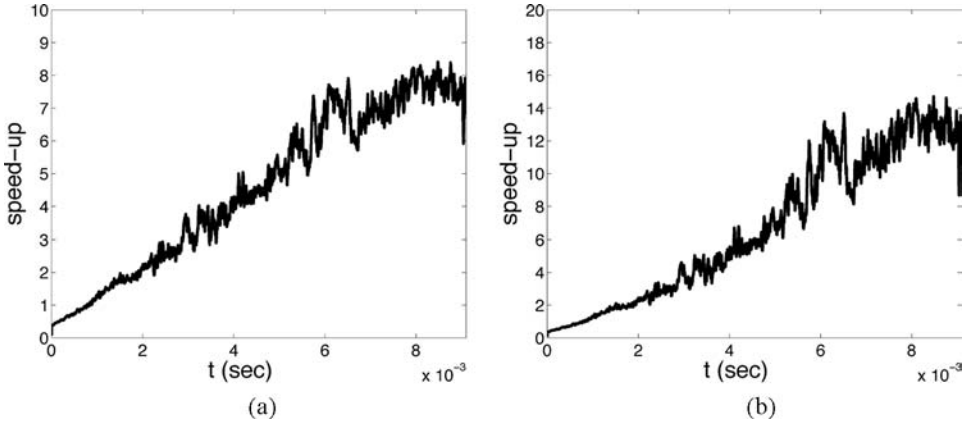

Figure 11. Speed-up (equation (35)) achieved by ISAT. Results obtained with $\Delta t = 1.82 \times 10^{-7}$ s, $\varepsilon_{\text{tol}} = 10^{-7}$, and $\varepsilon_{\text{abs}} = \varepsilon_{\text{rel}} = 10^{-10}$. (a) Overall time step speed-up, (b) speed-up for the reaction sub-step.

construction speed-up factor being approximately 12–14. Note here that the speed-up factors continue an upward trend due to the increasing CPU time required by the DVODE scheme.

Finally, in addition to the ISAT performance characteristics discussed above, it is appropriate to consider the computer memory requirements necessary to store the ISAT table. For the present calculations, which access a relatively small portion of reaction phase space, the ISAT table contains approximately 6150 entries and requires approximately 310 megabytes of storage.

4.6 *Further discussion*

4.6.1 Chemical mechanisms. In addition to the methane–air test problem described above, a similar problem was run for the case of hydrogen-air using the nine species and 19 reaction detailed chemical mechanism used in Maas and Pope [33]. For the case of the hydrogen–air mechanism, convergence and accuracy studies demonstrate similar results. In particular, second-order temporal convergence is observed and it is found that ε_{tol} controls tabulation error and overall scheme accuracy. Performance characteristics are, however, notably different than the case of methane–air. For the hydrogen–air mechanism, following the initial ISAT table build phase, the overall speed-up factor is approximately 1.5 while the reaction sub-step speed-up factor is approximately 2.75. The difference between these results and those presented here for the methane–air case are attributed, in part, to the size and complexity differences of the two mechanisms. A greater ISAT speed-up is observed for the methane case because it takes more CPU time for DVODE to complete the reaction sub-steps; the amount of CPU time required increases due to the increased number of species, chemical reactions, and associated system stiffness. For ISAT, however, the table retrieve time increases as n_s^2 and is independent of the number of reactions and system stiffness introduced by the kinetic mechanism. Therefore, following the initial ISAT table build phase, table retrieves exhibit greater CPU time savings over DVODE for large chemical mechanisms. We anticipate even greater speed-ups than those observed here for mechanisms involving yet more species, reactions, and stiffness.

4.6.2 Random ISAT calling. During the table construction phase of the ISAT calculations, it is computationally advantageous that the binary tree which stores the table entries be well-balanced, i.e. that it grows such that different branches of the tree have roughly equal lengths. To facilitate this construction, the reaction sub-steps are performed in a random

spatial order. There is minimal additional computational cost associated with incorporation of randomness as a random order must only be generated once per time step.

4.6.3 Speed-up limitations. The incorporation of ISAT into the predictor/corrector algorithm is designed to accelerate the calculation of the reaction sub-steps. Consequently, CPU time spent outside of the reaction sub-steps is not decreased by the use of ISAT. If a relatively large portion of the per-step CPU time is spent outside of the reaction sub-steps (e.g. as a result of detailed transport models), then the speed-up factor may be lower than those observed here. In future work we intend to incorporate detailed transport models (e.g. mixture-averaged) into the calculations and report our findings. Regardless, the presence of ISAT is expected to reduce the total amount of CPU time required to perform the calculations.

5. Conclusions

This work has focused on the inclusion of ISAT in the operator-splitting scheme of Najm and Knio [2]. To do so, a Strang sub-splitting method is introduced which further separates the reaction processes from transport processes. For the pure reaction sub-steps, the adaptive tabulation scheme ISAT is used which makes use of a stiff ODE solver. The non-stiff equations in the sub-splitting scheme are computed using a single-stage, second-order Runge–Kutta scheme. The scheme is then applied to a one-dimensional laminar premixed methane–air flame propagation problem with detailed chemistry. For this problem, second-order temporal convergence is demonstrated and results are compared with those obtained using the algorithm in [2]. The impact of the ISAT error tolerance on solution accuracy is demonstrated and it is shown that solution error can be controlled by changing the ISAT tolerance. Finally, the CPU time savings obtained by using ISAT rather than direct integration (DVODE) is examined. It is found that with GRIMech3.0, after an initial ISAT table build-up, the use of ISAT speeds the reaction sub-steps of the computations by roughly a factor of 13 and the overall scheme achieves a speed-up of approximately 7.5. For problems involving more complex chemistry and flow conditions, greater speed-ups are anticipated. On the other hand, less speed-up is anticipated when portions of the algorithm not presently tabulated with ISAT, e.g. transport property evaluation, involve more complex CPU-intensive computations. In this case, we can pursue tabulation of these terms to regain speed-up.

Acknowledgments

MAS acknowledges support from a NASA Graduate Student Researchers Program Fellowship and the Langley Research Center. SBP acknowledges support from the U.S. Department of Energy Grant No. DE-FG02-90ER14128. HNN has been supported by the U.S. Department of Energy (DOE), and by the DOE Office of Basic Energy Sciences (BES), Division of Chemical Sciences, Geosciences and Biosciences. Computations were performed at Sandia National Laboratories. Sandia National Laboratories is a multiprogram laboratory operated by Sandia Corporation, a Lockheed Martin Company, for the United States Department of Energy under contract DE-AC04-94-AL85000.

References

[1] Pope, S.B., 1997, *Combust. Theory Modelling*, **1**, 41.
[2] Najm, H.N. and Knio, O.M., 2004, *J. Sci. Comp.*, *in press*.

[3] Fiorina, B., Baron, R., Gicquel, O., Thevenin, D., Carpentier, S., and Darabiha, N., 2003, *Combust. Theory Modelling*, **7**, 449.
[4] Schwer, D.A., Lu, P., and Green, Jr., W.H., 2003, *Combust. Flame*, **133**, 451.
[5] Tonse, S.R., Moriarty, N.W., Brown, N.J., and Frenklach, M., 1999, *Israel Journal of Chemistry*, **39**, 97.
[6] Tonse, S.R., Moriarty, N.W., Frenklach, M., and Brown, N.J., 2003, *Int. J. Chem. Kinetics*, **35**, 438.
[7] Bell, J.B., Brown, N.J., Day, M.S., Frenklach, M., Grcar, J.F., Propp, R.M., and Tonse, S.R., 2000, *Proc. Combust. Inst.*, **28**, 107.
[8] Kim, J. and Cho, S.Y., 1997, *Atmos. Environ.*, **31**, 2215.
[9] Lanser, D. and Verwer, J.G., 1999, *J. Comput. Appl. Math.*, **111**, 201.
[10] Schwer, D.A., Lu, P., and Green, Jr., W.H., and Semião, V., 2003, *Combust. Theory Modelling*, **7**, 383.
[11] Najm, H.N. and Wyckoff, P.S., 1997, *Combust. Flame*, **110**, 92.
[12] Najm, H.N., Wyckoff, P.S., and Knio, O.M., 1998, *J. Comput. Phys.*, **143**, 381.
[13] Knio, O.M., Najm, H.N., and Wyckoff, P.S., 1999, *J. Comput. Phys.*, **154**, 428.
[14] Day, M.S. and Bell, J.B., 2000, *Combust. Theory Modelling*, **4**, 535.
[15] Bell, J.B., Day, M.S., and Grcar, J.F., 2002, *Proc. Combust. Inst.*, **29**, 1987.
[16] Bell, J.B., Day, M.S., Rendleman, C.A., Woosley, S.E., and Zingale, M.A., 2004, *J. Comput. Phys.* **195**, 677.
[17] Yang, B. and Pope, S.B., 1998, *Combust. Flame*, **112**, 85.
[18] Singer, M.A. and Pope, S.B., 2004, *Combust. Theory Modelling*, **8**, 361.
[19] Rehm, R.G. and Baum, H.R., 1978, *NBS J. Res.*, **83**, 297.
[20] Majda, A. and Sethian, J., 1985, *Combust. Sci. Technol.*, **42**, 185.
[21] Kee, R.J., Coltrin, M.E., and Glarborg, P., 2003, *Chemically Reacting Flow* (New Jersey: John Wiley & Sons, Inc.).
[22] Verwer, J.G., 1996, *App. Num. Math.*, **22**, 359.
[23] Caracotsios, M. and Stewart, W.E., 1985, *Comput. Chem. Eng.* **9**, 359.
[24] Brown. P.N., Byrne, G.D., and Hindmarsh, A.C., 1989, *SIAM J. Sci. Stat. Comput.*, **10**, 1038.
[25] Ascher, U.M. and Petzold, L.R., 1998, *Computer Methods for Ordinary Differential Equations and Differential-Algebraic Equations* (Philadelphia, PA: SIAM).
[26] Smith, G.P., Golden, D.M., Frenklach, M., Moriarty, N.W., Eiteneer, B., Goldenberg, M., Bowman, C.T., Hanson, R.K., Song, S., Gardiner, Jr., W.C., Lissianski, V.V., and Qin, Z., http://www.me.berkeley.edu/gri_mech/.
[27] Kee, R.J., Grcar, J.F., Smooke, M.D., and Miller, J.A., 1985, *Sandia Report SAND85-8240 Sandia National Laboratories*, Livermore, CA.
[28] Kee, R.J., Rupley, F.M., and Miller, J.A., 1989, *Sandia Report SAND89-8009 Sandia National Laboratories*, Livermore, CA.
[29] Najm, H.N., Paul, P.H., Mueller, C.J., and Wyckoff, P.S., 1998, *Combust. Flame*, **113**, 312.
[30] Turns, S.R., 2000, *An Introduction to Combustion* (McGraw-Hill, USA).
[31] Poinsot, T. and Veynante, D., 2001, *Theoretical and Numerical Combustion* (Philadelphia, PA: R.T. Edwards).
[32] Poinsot, T., Echekki, T., and Mungal, M.G., 1991, *Combust. Sci. Technol.*, **81**, 45.
[33] Maas, U. and Pope, S.B., 1992, *Combust. Flame*, **88**, 239.